SINTERING, MICROSTRUCTURE, AND MECHANICAL PROPERTIES OF A GLAZE. EFFECT OF KAOLIN ADDITION.

E. Blasco, J. L. Amorós, C. Feliu, A. Moreno

Group for glazes and whiteware sinter-crystallisation. Instituto de Tecnología Cerámica (ITC). Asociación de Investigación de las Industrias Cerámicas (AICE). Universitat Jaume I. Castellón. Spain.

ABSTRACT

The study examines the effect of kaolin addition to a frit of the SiO_2–Al_2O_3–RO (R=Ca, Mg, Sr) system, which devitrifies anorthoclase and diopside, on sinter-crystallisation at constant-rate heating, microstructure, and microhardness of the material. Differential scanning calorimetry (DSC) and hot stage microscopy (HSM) revealed that, as kaolin content and heating rate increased, crystallisation shifted to higher temperatures. The sintering process of the frit, except at high heating rates, and of the frit mixtures with kaolin developed in two stages: in the first, sintering developed by viscous flow of the material before crystallisation began; in the second, by viscous flow of the mixture: residual glass–devitrified phases. Test specimens were prepared by pressing and fired at a heating rate of 15K/min to different maximum temperatures, with a 6min dwell at that temperature. In addition to the usual technological properties, fired test specimen microstructure, open and closed porosity, pore size distribution, and microhardness were determined. As kaolin content increased, the temperature at which the piece reached maximum densification rose; linear firing shrinkage decreased; and test specimens were obtained from the frit and from the frit plus 8% kaolin by weight with low closed porosity (≈3–4%) and high microhardness (≈12GPa). The microhardness results were interpreted on the basis of the microstructural characteristics of the resulting materials.

1. INTRODUCTION

Application of the sinter-crystallisation technology, which involves frit densfication and subsequent devitrification with a single thermal treatment, enables materials of a glass-ceramic nature with good mechanical properties to be obtained on applying thermal cycles similar to those used in the ceramic floor and wall tile industry. This process can also be applied on adding moderate amounts of other additives to the frit and when crystallisation partially overlaps densification. In previous papers, using a frit based on the SiO_2–Al_2O_3–RO (R=Ca, Mg, Sr) system, the effect of frit particle size and heating rate on the nature of the devitrifying phases and on their sintering and crystallisation kinetics was studied [1][2][3]. When appropriate heating rates were applied, the sinter-crystallisation process yielded pore-free materials that devitrified anorthoclase and diopside. In addition, the crystallisation mechanism was superficial, so that starting frit particle size largely determined sintering and crystallisation process kinetics and resulting crystal size.

A recent study [4] examined the effect of kaolin on the sinter-crystallisation kinetics of this frit, with regard to its possible use as a major component in a glaze or in large slabs that exhibit better mechanical properties than those obtained at present using traditional compositions. This paper summarises the results of a more extensive study in which the technological properties, microstructure, and microhardness of materials prepared from the above frit and its kaolin additions, fired at different temperatures, were determined.

2. EXPERIMENTAL PROCEDURE

The study was conducted on a frit (F) with the following mole composition: SiO_2 (60), Al_2O_3 (12), RO (22), and R_2O (6). Frit particle size distribution matched that customarily used in industrial practice [4]. Mixtures were prepared by the wet method, adding 8% (F8) and 16% (F16) by weight of kaolin for industrial use. The frit and its dried mixtures were used to prepare test specimens, 2cm in diameter and 5mm thick, by pressing at 30MPa and 5% moisture content. Water absorption, WA (%), linear shrinkage, LS, and bulk density, ρ_{AP}, were determined in accordance with standard methods. The degree of sintering progress, X, was determined from the expression:

$$X = \frac{ln(S_0/S)}{ln\,(S_0/S_{min})} \qquad \text{Eq. 1}$$

where S_0, S, and S_{min} are the areas of the initial, instantaneous, and minimum test specimen silhouette, obtained by hot stage microscopy (HSM) at different heating rates.

Crystallisation kinetics was studied by scanning differential calorimetry (DSC). The nature of the devitrifying phases was determined by X-ray diffraction (XRD). Pore size distribution, pore number density per unit surface area, N, and total porosity, ε, were determined by scanning electron microscopy (SEM) and image analysis. The minimum number of pores measured in each sample was 4000. Pore size was calculated as the diameter of the circle whose area coincided with that of the measured pore. Pore size distributions were determined by number and by volume. The average size of a series of j pores, d_{av}, was calculated from the following equation:

$$d_{av} = \frac{1}{j}\sum_{i=1}^{i=p} d_i \qquad \text{Eq. 2}$$

Total porosity, ε, was calculated as the ratio: total pore area/pore area + solid area. Open porosity, ε_{open}, was determined as the product of bulk density and water absorption. For each test specimen, the uncertainty of each parameter was calculated as the standard deviation of the values obtained in each of the images. Microhardness was determined by nano-indentation, using a Berkovich diamond indenter. Thirty-six nano-indentations were made in the polished section of each test specimen, with a maximum load of 1N and distance between imprints of 50μm. The results were fitted to the Weibull model [5]:

$$F(H) = 1 - exp\left[-ln2\left(\frac{H}{H_M}\right)^m\right] \qquad \text{Eq. 3}$$

where F(H) is the distribution function in cumulative form, H_M the mean hardness value, and m the uniformity index.

3. RESULTS

3.1. SINTER-CRYSTALLISATION OF MATERIALS. EFFECT OF KAOLIN CONTENT AND HEATING RATE.

XRD revealed (Figure 1) that anorthoclase was the major phase in every composition. As kaolin content increased, the amount of diopside that devitrified decreased until practically cancelling out in the F16 test specimen. These results confirm those obtained in previous studies [4].

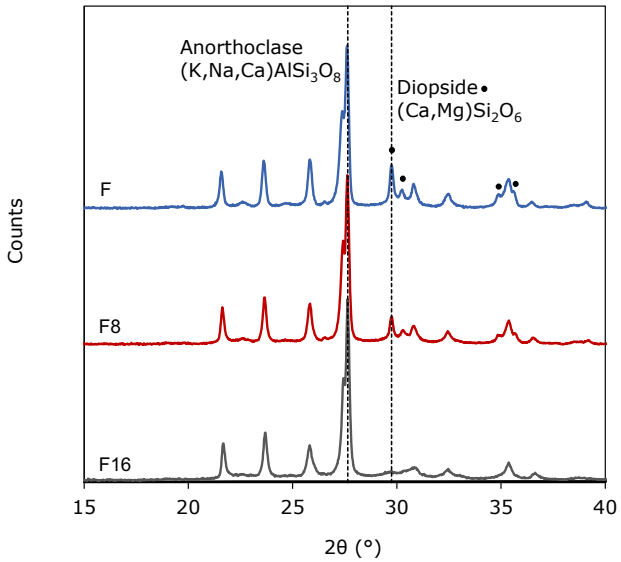

Figure 1. *XRD diffractogram corresponding to test specimens F, F8, and F16 fired at 1100 ºC. Heating rate 15K/min and 6min dwell.*

The DSC curves corresponding to the frit (F) exhibited a double exothermic peak corresponding to overlapping anorthoclase and diopside crystallisation between 900 ºC and 1000 ºC (Figure 2a). With the kaolin addition, the peak shifted towards higher temperatures and became more symmetrical, developing a sharp, symmetrical peak in F16, in which diopside no longer crystallised. In addition, the endothermic peak relating to the melting of devitrifying crystals was larger and better defined in F than in the other compositions (T_m in Figure 2). The sintering process in frit F (Figure 2a) had been practically completed at crystallisation onset, so that the sintering curve, X versus T, could practically be described by a single stage. However, as kaolin content rose (Figure 2b), the two processes increasingly overlapped, so that the sintering curve, X vs T, contained two stages: the first relating to viscous flow sintering of the starting material and the second, also involving viscous flow sintering, but of the mixture of residual glass–devitrified crystalline phases. This behaviour was caused by the kaolin particles that surrounded the frit particles, which reduced frit particle contact surface and thus adversely affected crystallisation and sintering. Indeed, both processes were delayed by the increase in kaolin content.

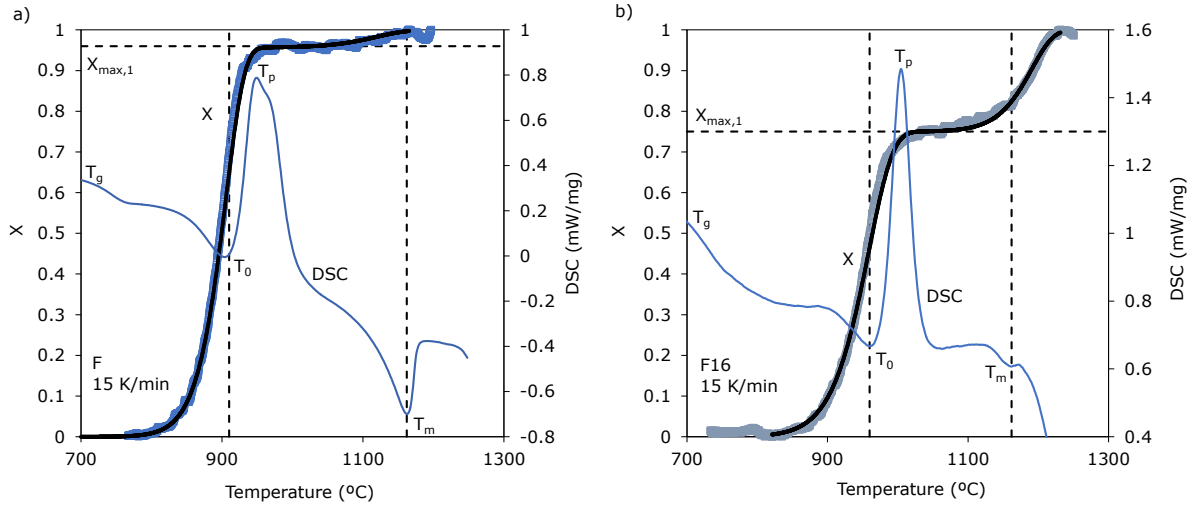

Figure 2. *Sintering (X versus Temperature) and crystallisation (DSC) curves obtained at a heating rate of 15K/min in F and F16. T_g, T_0, T_p, and T_m are the transformation, crystallisation onset, and maximum crystallisation and melting rate temperatures, respectively; $X_{max,1}$ is the maximum degree of crystallisation attained in sintering stage 1. Solid sintering curves, calculated in accordance with model [4].*

Figure 3 shows that, as the heating rate, β, and/or kaolin content increased, crystallisation onset temperature, T_0, and maximum crystallisation rate temperature, T_p, rose. This effect was of a logarithmic type (Figure 3a). In contrast, melting temperature, T_m, was independent of kaolin content and depended very little on heating rate, β. Moreover, when the heating rate decreased and/or kaolin content increased, the degree of overlap between the crystallisation and sintering processes grew (Figure 3b and c). Generally speaking, at low heating rates (β=5K/min), all samples clearly exhibited a temperature range in which sintering halted as a result of frit crystallisation, which led to higher maximum densification temperatures than those obtained at higher heating rates (50K/min). This behaviour stemmed from the effect of heating rate on crystallisation being greater than on viscous flow sintering. At high heating rates (Figure 3c), both frit, F, and its mixture with 8% kaolin by weight, F8, sintered before the crystalline phases devitrified, which led to a very low maximum densification temperature.

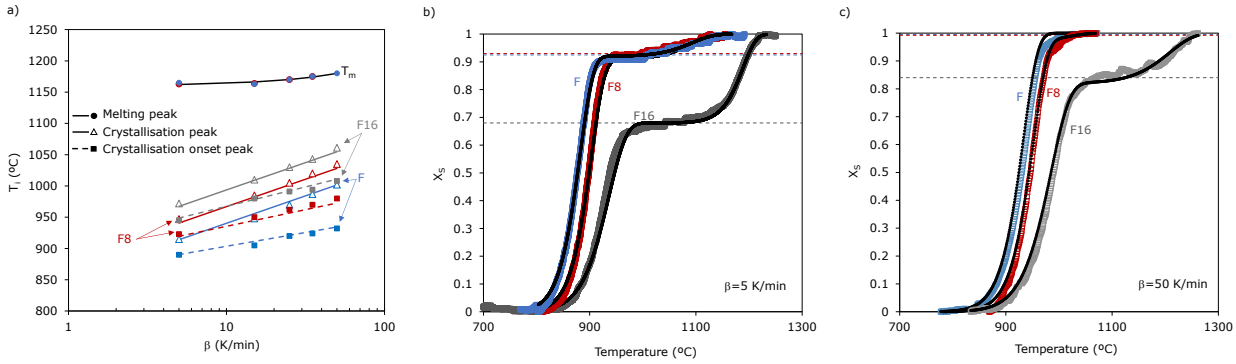

Figure 3. *Combined effect of kaolin content and heating rate on: a) crystallisation; and b) and c) sintering. Solid sintering curves, calculated in accordance with the model [4].*

3.2. EVOLUTION OF MICROSTRUCTURE WITH FIRING TEMPERATURE

At 900 ºC, frit F (Figure 4) exhibited incipient surface crystallisation at the edges of already sintered frit particles; between 900 ºC and 1100 ºC, crystalline phase content increased and crystal size grew. From this temperature on, anorthoclase content decreased and diopside completely dissolved. Small, irregularly shaped pores were observed at all temperatures between the crystals, mainly relating to diopside crystallisation. These crystallisation-induced pores developed because diopside crystal density was much greater than that of the glass from which the diopside crystals originated [4].

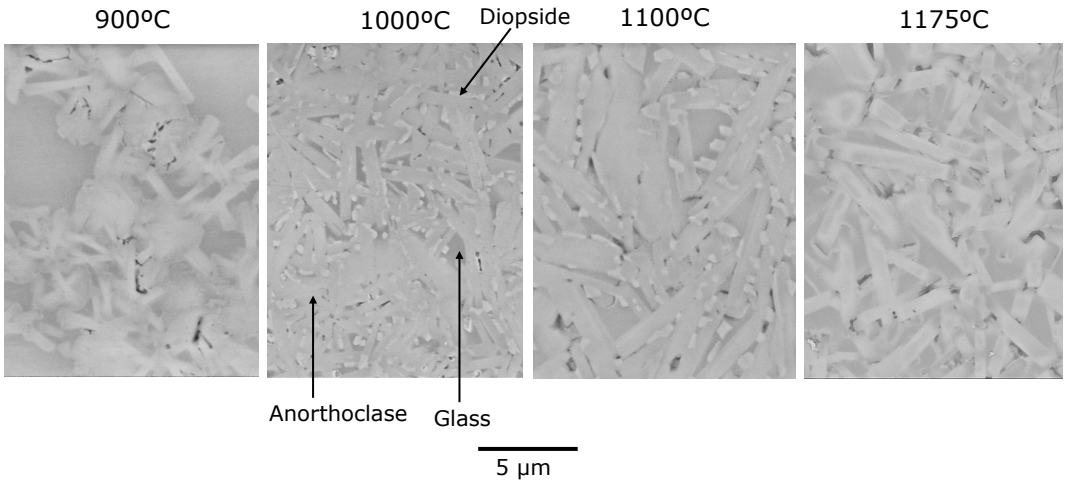

Figure 4. *Evolution of frit F microstructure with firing temperature (heating rate 15K/min and 6min dwell).*

Mixtures F8 and F16 exhibited analogous behaviour with regard to crystalline phase growth with temperature. However, when kaolin content increased, the amount of crystalline phases decreased, particularly diopside, which no longer crystallised in F16 (Figure 5). Induced crystallisation porosity also decreased as kaolin content rose. Obviously, in F16, in which no diopside crystallised, induced crystallisation porosity was not observed either.

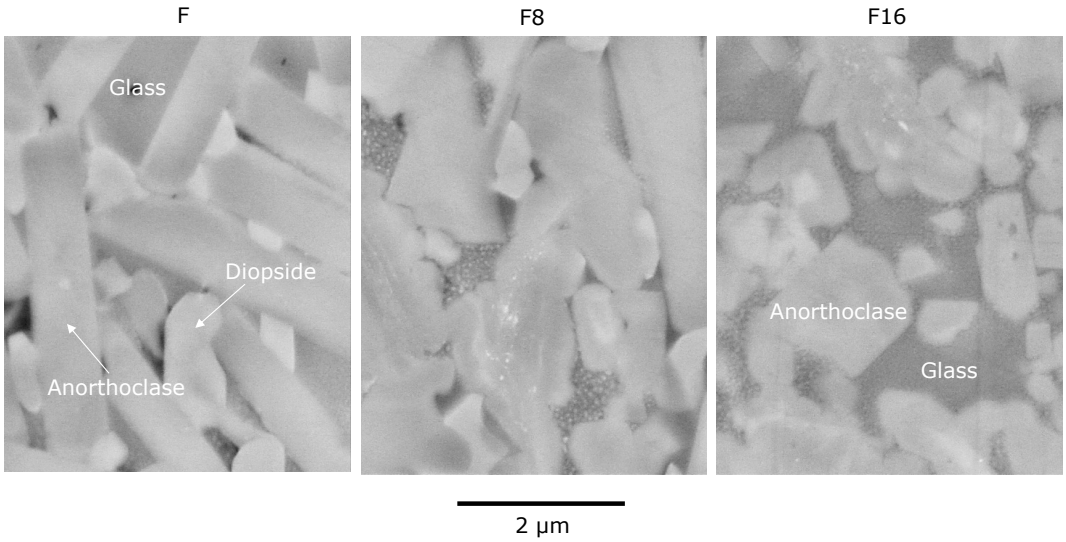

Figure 5. *Effect of kaolin content on the microstructure of samples F, F8, and F16 fired at 1100 ºC (heating rate 15K/min and 6min dwell).*

The pore size distributions (PSDs) were determined by area and by number. These results are plotted for F and F16 in Figure 6. In frit F, in which porosity in the studied temperature range was closed, the following may be observed: i) the PSDs expressed by number shifted towards smaller pore sizes than those calculated by area; ii) between 900 ºC and 1100 ºC, porosity and the number of pores smaller than 1µm, induced by crystallisation, increased markedly. The curve segments higher than 1µm remained practically unchanged up to 1100 ºC; iii) at 1175 ºC, when diopside had already completely dissolved and anorthoclase had partially dissolved in the glass phase, the number of pores smaller than 1µm decreased and the number of larger-sized pores increased. Sample F16 exhibited the typical behaviour observed in sintering glasses and glass–crystalline phase composites [6][7]. That is, as temperature rose, porosity decreased and pore removal was sequential: the smallest pores disappeared first, followed by the larger ones. For this mixture, porosity was higher and essentially open, as may be observed in Figure 7.

For the frit and its mixtures, the variation with firing temperature was determined of pore number density, N; total porosity, ε, and open porosity, ε_{open}; and average pore diameter, d_{av}, (Figure 8). These results confirmed those obtained previously. Indeed, for frit F, pore number density, N, increased on going from 900 ºC to 1000 ºC, owing to the formation of induced crystallisation porosity, and N practically remained steady between 1000 ºC and 1100 ºC. At 1175 ºC, owing to the disappearance of crystalline phases and pore size growth, N decreased considerably. Total porosity, ε, which was closed, remained practically constant between 1000 ºC and 1175 ºC. In sample F16, up to 1000 ºC, porosity was essentially open, ε_{open}, as Figure 7 shows. Total porosity, ε, and pore number density, N, decreased as temperature rose, while average pore size, d_{av}, increased. Such behaviour, simultaneously involving pore growth with a reduction in porosity, ε, and in pore number density, N, is typical in sintering glass–crystalline phase composites [6][7]. Sample F8 exhibited an intermediate behaviour.

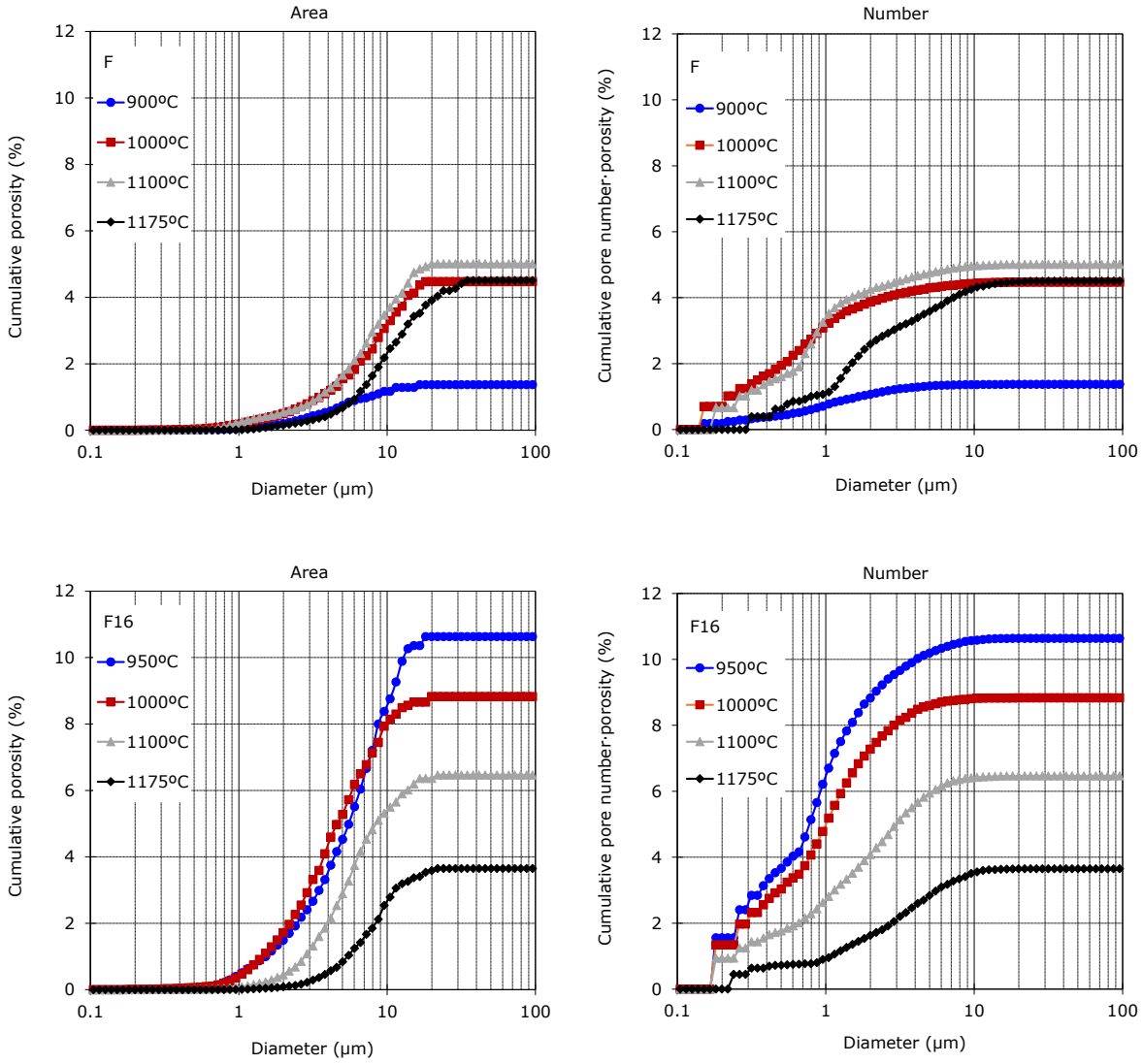

Figure 6. *Evolution with firing temperature of pore size distribution in cumulative form, by area and by number, of frit F and mixture F16 (heating rate 15K/min and 6min dwell).*

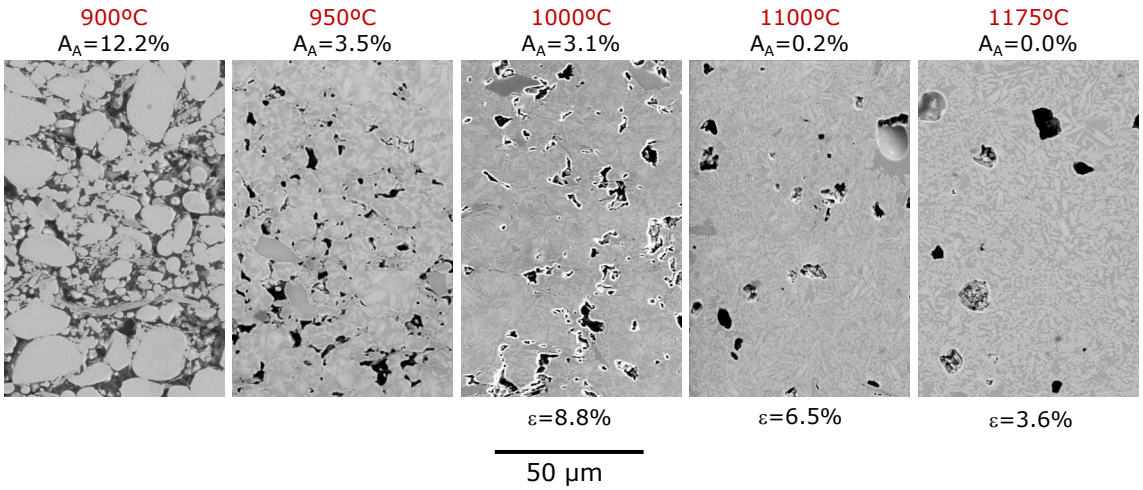

Figure 7. *Evolution of sample F16 microstructure with firing temperature (heating rate 15K/min and 6min dwell).*

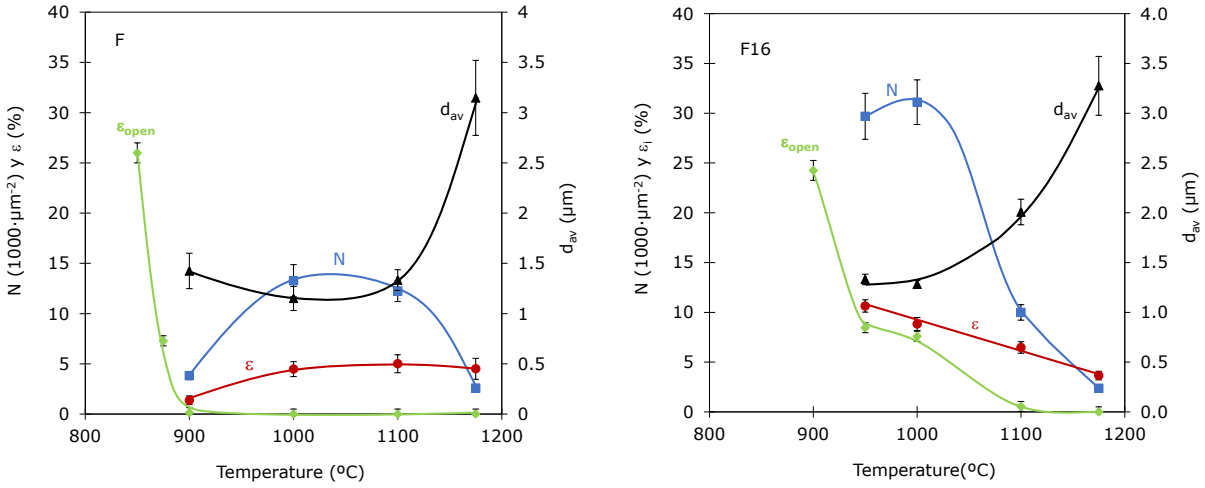

Figure 8. *Evolution with firing temperature of pore number density, N, total porosity, ε, open porosity, ε_{open}, and average pore diameter, d_{av}, (heating rate 15K/min and 6min dwell).*

3.3. MICROHARDNESS OF THE MATERIALS. RELATIONSHIP WITH MICROSTRUCTURE.

Microhardness was determined by nano-indentation of polished sections of the test specimens fired at 1000 ºC, 1100 ºC, and 1175 ºC. The mean values and standard deviation (error bars) corresponding to each test specimen have been plotted in Figure 9a. Sample F8 and F16 microhardness increased with firing temperature, owing to a parallel decrease in sample porosity. The values corresponding to sample F16 were lower than those of F8; this was mainly due to lower crystalline phase content. In contrast, sample F hardness peaked at 1100 ºC. This was because the crystal mass fraction was highest at this temperature (1100 ºC), while its porosity was practically the same at the three temperatures.

The cumulative microhardness distribution for test specimens F, F8, and F16, fired at the optimum temperature, is shown in Figure 9b. The solid curves correspond to the fit of the experimental data (symbols) to the Weibull model (Eq. 3). In every case, the uniformity index, m, exhibited a high value, as did mean hardness, H_M, the latter being much higher than that exhibited by different glass–crystalline phase composites and ceramic glazes [5][8][9]. In many experimental microhardness distributions, a certain bimodal behaviour may be observed, in which the low hardness values may be explained as the result of test specimen porosity. To verify this, the distribution curves that exhibited a bimodal behaviour were fitted to the sum of two Weibull distributions (Figure 10). In addition, the material volume sensitive to indentation (VSI) was calculated as a semi-sphere with a radius equal to 3–5 times maximum indentation depth [5][10][11]. By way of example, a possible indentation measurement distribution with its corresponding VSIs has been plotted in Figure 10. It shows the presence of pores of different size, totally or partially included in the VSIs (dashed circles). The hardness values of these indentations corresponded to the Weibull curve of low hardness values; regarding the rest, most would correspond to pore-free VSIs (continuous circles) and constitute the Weibull curve segment of greatest hardness. Therefore, a reduction in sample porosity would result in the elimination of low hardness values, which would increase the uniformity of this property, m, and its mean value, H_M.

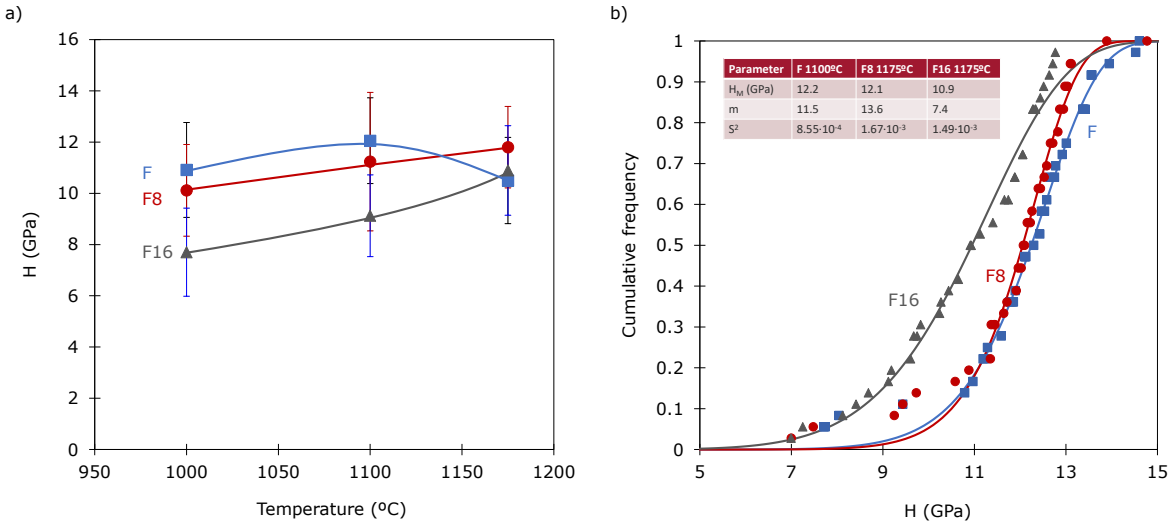

Figure 9. *Effect of kaolin addition on the microhardness of samples F, F8, and F16: a) average values and standard deviation (error bars) of the test specimens fired at 1000 ºC, 1100 ºC, and 1175 ºC; b) cumulative microhardness distribution for the test specimens fired at their optimum temperature. Fit of experimental data (symbols) to the Weibull model (solid curves). Heating rate 15K/min and 6min dwell.*

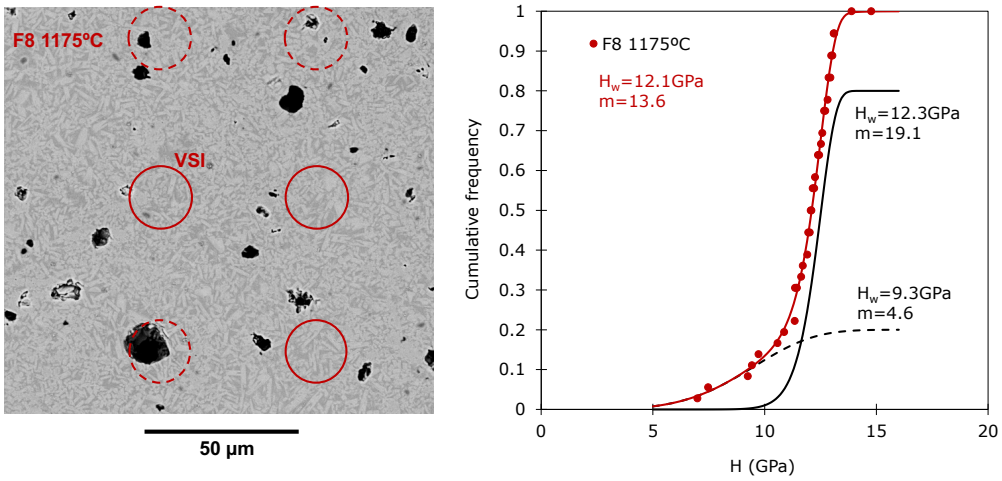

Figure 10. *Fit of the bimodal distribution of the experimentally determined microhardness (symbols) to the sum of two Weibull distributions (curves). Model of the VSI distributions and their overlap with pores.*

4. CONCLUSIONS

Increasing kaolin content decreased the amount of crystalline phases (anorthoclase and diopside) that devitrified in a frit of the SiO_2–Al_2O_3–RO (R=Ca, Mg, Sr) system. The addition of 16% kaolin by weight to this frit prevented diopside formation. Increasing the kaolin content and/or heating rate shifted sintering and crystallisation of the material towards higher temperatures. The degree of overlap of both processes increased as the heating rate decreased and kaolin content increased so that, at high heating rates and low kaolin contents, denser pieces were obtained at low firing temperature.

The variation of the microstructure of the frit and of its mixtures with kaolin with firing temperature was determined. The frit led to the formation of induced crystallisation porosity, owing to the greater density of diopside than that of the glass from which it devitrified. In the temperature range between 1000 ºC and 1175 ºC, frit porosity was low, closed, and remained practically constant. On raising kaolin content, induced crystallisation porosity decreased until it cancelled out at 16% kaolin by weight. The porosity of the mixtures fired in this range of temperatures decreased with this variable to low values (≈3–4%) at 1175 ºC. For all the studied compositions, an increase in maximum firing temperature led to average pore size growth.

Microhardness increased with crystalline phase content and/or with lower porosity. The microhardness distribution curve was fitted to the Weibull model. Samples F and F8, fired at 1100 ºC and 1175 ºC, yielded materials with low closed porosity (≈3–4%), high microhardness (>12GPa), and high hardness uniformity indexes (m>11). The abnormally low individual microhardness values observed in some test specimens stemmed from the overlap of the material volume sensitive to indentation, VSI, with pores.

5. REFERENCES

[1] J. L. Amorós, E. Blasco, A. Moreno, N. Marín, C. Feliu. Sinter-crystallisation kinetics of a SiO_2–Al_2O_3–CaO–MgO–SrO glass-ceramic glaze. Journal of Non-Crystalline Solids, 532, 119900, 2020.

[2] J. L. Amorós, E. Blasco, A. Moreno, N. Marín, C. Feliu. Effect of particle size distribution on the sinter-crystallisation kinetics of a SiO_2–Al_2O_3–CaO–MgO–SrO glass-ceramic glaze. Journal of Non-Crystalline Solids, 542, 120148, 2020.

[3] J. L. Amorós, E. Blasco, C. Feliu, A. Moreno. Effect of particle size distribution on the evolution of porous, microstructural, and dimensional characteristics during sinter-crystallisation of a glass-ceramic glaze. Journal of Non-Crystalline Solids, 572, 121093, 2021.

[4] J. L. Amorós, E. Blasco, C. Feliu, A. Moreno. Effect of kaolin addition on the sinter-crystallisation kinetics of compacts of a crystallising frit. Journal of Non-Crystalline Solids, 596, 121864, 2022.

[5] J. L. Amorós, E. Blasco, A. Moreno, C. Feliu, A. O. Boschi, N. Marín. Improvement of the mechanical and aesthetic properties of a coating by inkjet technology. International Journal of Applied Ceramic Technologies, 18, 937–946, 2021.

[6] J. L. Amorós, E. Blasco, A. Moreno, E. Zumaquero, C. Feliu. Non-isothermal sintering of powdered vitrified composites. A kinetic model. Materials Letters, 236, 236–239, 2019.

[7] J. L. Amorós, A. Moreno, E. Blasco. Viscous flow sintering in glass matrix composites with rigid inclusions. Ceramics in Modern Technologies, 3, 155–162, 2019.

[8] J. L. Amorós, E. Blasco, A. Moreno, C. Feliu. Mechanical properties obtained by nanoindentation of sintered zircon-glass matrix composites. Ceramics International, 46, 10691–10695, 2020.

[9] F. N. Bertan, O. R. K. Montedo, C. R. Rambo, D. Hotza, A. P. Novaes de Oliveira. Extruded ZrSiO4 particulate-reinforced LZSA glass-ceramics matrix composite. Journal of Materials Processing Technology, 209, 1134–1142, 2009.

[10] G. Constantinides, K. S. Ravi Chandran, F. J. Ulm, K. J. Van Vliet. Grid indentation analysis of composite microstructure and mechanics: principles and validation. Materials Science and Engineering: A, 1–2(430), 189–202, 2006.

[11] P. L. Larsson, A. E. Giannakopoulos, E. Söderlund, D. J. Rowcliffe, R. Vestergaard. Analysis of Berkovich indentation. International Journal of Solids and Structures, 2(33), 221–248, 1996.